Available online at www.sciencedirect.com
SCIENCE DIRECT®
International Journal of Mass Spectrometry 230 (2003) 151–159
International Journal of Mass Spectrometry
www.elsevier.com/locate/ijms

Differentiation of isomeric oxygenated adsorbates using low-energy ion/surface collisions

Nathan Wade, Sung-Chan Jo, Bogdan Gologan, R. Graham Cooks*

Department of Chemistry, Purdue University, West Lafayette, IN 47907, USA

Received 10 July 2003; accepted 18 August 2003

For John Beynon, on his 80th birthday, in appreciation of the opportunities he provided to participate in so much exciting science

Abstract

Reactive scattering of polyatomic ions in the hyperthermal collision energy range (<100 eV) is used to distinguish isomeric oxygenated adsorbates and to quantify their relative amounts when co-adsorbed at a surface. The self-assembled monolayers (SAMs) of interest are constructed from HO-terminated, CH_3O-terminated, and CH_3CH_2O-terminated dialkyl disulfides. Projectile ions used for ion/surface scattering experiments include CF_3^+, $SiCl_3^+$, and the molecular ion of pyridine, $C_5H_5N^{\bullet+}$. Each of these ions exhibits a unique scattered ion profile upon collision with the SAM monolayer surfaces, and so provides different information about the surfaces. Hydrogen atom abstraction by the $C_5H_5N^{\bullet+}$ ion is more prominent at the CH_3CH_2O- and CH_3O-terminated surfaces than the HO-terminated surface, while collisions of $SiCl_3^+$ yield reactively scattered products which reflect the chemical composition of these surfaces. For instance, $SiCl_2OH^+$ and $SiCl_2OCH_3^+$ are scattered from the HO-terminated and CH_3O-terminated surfaces, respectively. Ion/surface collisions involving the CF_3^+ ion produce chemically sputtered ions from the oxygenated adsorbates, which are valuable for quantitation of those groups. Preferential sputtering of the CH_3O-terminated versus the HO-terminated SAM surface is ascribed to favored thermochemistry and the more accessible CH_3O-terminated adsorbate. Fundamental ion/surface scattering processes, such as inelastic collisions leading to surface-induced dissociation (SID), ion/surface reaction, and chemical sputtering are examined over a range of collision energies for each of the ion/surface types mentioned, and their value in surface analysis is demonstrated.

Keywords: Ion/surface collision; Self-assembled monolayer; Surface analysis; Reactive scattering; Surface-induced dissociation

1. Introduction

John Beynon reported activation of projectile ions by colliding ions with a stainless steel target in an ion kinetic energy spectrometer [1]. This early mass spectrometric study of ion/surface collisions is just one of many areas of mass spectrometry in which John Beynon made seminal contributions. Collisions of ions with surfaces in the hyperthermal collision energy range (<100 eV) represent a subject that has contributed to the elucidation of ion structure [2,3], the chemical analysis of surfaces [4,5], and the preparation of chemically modified surfaces [6,7]. Apart from these and other potential applications, attention has also been attracted to this area because of the variety and diversity of the processes involved, namely surface-induced dissociation (SID), ion/surface reactions, and chemical sputtering of surface molecules as gas-phase ions.

Surface-induced dissociation is the term used to describe the process of ion activation and subsequent fragmentation, which occurs when ions are allowed to collide inelastically with surfaces. When performed in the hyperthermal collision energy range, SID provides similar or greater internal excitation of the ion than its gas-phase counterpart, collision-induced dissociation (CID) [8,9]. The large, yet easily controlled internal energy deposition is useful for inducing fragmentation of large or stable molecules, especially biological ions [10]. The efficiency of ion activation achieved in SID has been shown to be dependent on the type of surface used as the target, with fluorocarbon surfaces being highly efficient both in terms of energy transfer and in terms of scattered ion yields [11]. The internal excitation achieved with fluorocarbon monolayer surfaces [12]

* Corresponding author. Tel.: +1-765-494-5263; fax: +1-765-494-9421.
E-mail address: cooks@purdue.edu (R.G. Cooks).

1387-3806/$ – see front matter © 2003 Elsevier B.V. All rights reserved.
doi:10.1016/j.ijms.2003.08.015

is significantly greater than that for hydrocarbon-covered surfaces [13]. Reasons suggested for the effectiveness of fluorocarbon surfaces over the other surfaces include the chemical inertness of these molecules, the larger ionization energy which suppresses neutralization, and the greater effective mass which increases momentum transfer [14].

Charge exchange involves electron transfer from the surface to the incoming projectile ion and occurs most efficiently when the recombination energy of the ion is equivalent to or exceeds the ionization energy of the molecular adsorbate on the surface. If this process is accompanied by sufficient energy transfer to the surface, ionized surface molecular fragments are released from the surface into the gas phase and can be observed in the scattered ion mass spectrum [15]. This process, known as chemical sputtering, is a useful way to characterize the chemical components present at the outermost layers of a surface [16].

Ion/surface reactions include events in which an atom or a group of atoms is transferred between the projectile ion and surface in the course of low-energy collisions, viz. they include the important process of reactive scattering. While large enough to cause dissociation of covalent bonds, the hyperthermal collision energies used in ion/surface scattering studies are not so large as to obscure the characteristic behavior of the ion/surface collision pair. Subsequent bond formation is often thermodynamically favored. Ion/surface collision products which retain a charge are observable by mass analysis and are referred to as reactively scattered ions. One of the earliest ion/surface reactions reported [17,18] involved the abstraction of hydrogen atoms from hydrocarbon surfaces by organic ions such as the molecular ions of benzene and pyridine. Heavier aromatic ions, such as the molecular ion of phenanthrene ($C_{14}H_{10}^{\bullet+}$), abstract alkyl groups as large as C_6H_n from hydrocarbon surfaces [19,20]. Other well-known ion/surface reactions involve C–C and C–F bond activation as a result of collisions of transition metal ions ($W^{\bullet+}$, $Cr^{\bullet+}$, and Re^+) [21], atomic ions (B^+, $Xe^{\bullet+}$, and I^+) [22,23], or polyatomic ions ($AlCl^+$ and PCl_2^+) [24] with fluorocarbon surfaces. The importance in chemistry of C–F bond activation and the role of ion/surface collisions in this process has been described recently by Mazurek and Schwarz [25].

Interest in reactive scattering is increased by the fact that it provides information on the nature of the surface. For example, adsorbed chlorobenzyl mercaptan isomers [5] can be differentiated based on reactions with $Cr^{\bullet+}$, which generate such product ions as $CrCl^+$ and $CrC_7H_6Cl^+$ with the accessible chlorine in the *p*-chloro isomer. In another study [26], the molecular ion of pyridine, $C_5H_5N^{\bullet+}$, was shown to allow distinction between 1,4-benzenedimethanethiol adsorbed on gold versus silver due to differences in the orientation of the adsorbates on the two metals.

A number of studies have revealed that selective chemical modifications can be performed at surfaces as a result of ion/surface reactions. Transhalogenation reactions [27] performed with reagents such as PCl_3^+ or $SiNCO^+$, have been shown to chemically transform terminal groups of fluorocarbon surfaces into terminal CF_2X units, where X represents a halogen atom or pseudohalogen group derived from the projectile ion [28]. Silicon nitride formation has been achieved by reactions of N^+ and $N_2^{\bullet+}$ ions with a Si(1 0 0) surface [29], and diamond-like carbon films have been formed at clean surfaces as a result of low-energy C^+ collisions [30]. Low-energy CF_3^+ and $C_3F_5^+$ ions have been used to modify a polystyrene surface, the $C_3F_5^+$ ion being more effective than the CF_3^+ ion [31].

Covalent addition of polyatomic cations at functionalized organic surfaces has also been demonstrated. Aromatic ions, such as the $(M - H)^+$ ion of chlorobenzene [6] covalently binds to a carboxylic acid terminated self-assembled monolayer surface through an ion/surface decarboxylation reaction, which is reminiscent of the condensed phase Kolbe reaction. Furthermore, hydroxy-terminated SAMs have been transformed into terminal esters [32] and silyl ethers [33] through reactions with such cations as the benzoyl cation, $C_6H_5CO^+$, and the trimethylsilyl cation, $Si(CH_3)_3^+$. The extent of such surface modifications produced by ion/surface reactions has been measured using X-ray photoelectron spectroscopy and Fourier transform infrared external reflectance spectroscopy (FTIR-ERS) [34].

In the present study, each of the above mentioned processes, viz. SID, ion/surface reactions, and chemical sputtering, contribute to the characterization and differentiation of three oxygenated surfaces. These surfaces studied are a hydroxy-terminated SAM (HO-SAM), a methoxy-terminated SAM (CH_3O-SAM), and an ethoxy-terminated SAM (CH_3CH_2O-SAM). Differences observed in the scattered ion products resulting from these surfaces provide insights into the characteristics and limitations of the fundamental processes observed in low-energy ion/surface collisions. Three different polyatomic cations, CF_3^+, $SiCl_3^+$, and $C_5H_5N^{\bullet+}$ are used as projectiles and their different properties help to accentuate the different ion/surface collision processes.

2. Experimental methods

2.1. Surface preparation

Synthesis of the HO-terminated dialkyl disulfide ($HO(CH_2)_{11}S\text{-})_2$ was performed by dissolving 11-mercapto-undecanol (Aldrich Inc., Milwaukee, WI) in an ethanolic solution of potassium hydroxide (10 mM KOH). Then 30% hydrogen peroxide was added and the solution was heated for 8 h while being stirred. The disulfide was extracted from water with diethyl ether and dried with anhydrous sodium sulfate. After removal of the solvent, the product was recrystallized from benzene. The HO-terminated disulfide was then used for synthesis of the CH_3O-terminated ($CH_3O(CH_2)_{11}S\text{-})_2$, CD_3O-terminated ($CD_3O(CH_2)_{11}S\text{-})_2$, and CH_3CH_2O-terminated ($CH_3CH_2O(CH_2)_{11}S\text{-})_2$ disul-

fides. Synthesis of the CH_3O-terminated disulfide was performed by dissolving the HO-terminated disulfide in tetrahydrofuran along with sodium hydride and methyl iodide. The reaction mixture was stirred and heated under reflux for 24 h. The desired product was extracted from water with dichloromethane, and then dried with anhydrous sodium sulfate. After removal of the solvent, the product was recrystallized from methanol and purified by flash chromatography using 1:4 ethyl acetate/hexanes as the mobile phase. The same procedure was used for synthesis of the CD_3O-terminated and CH_3CH_2O-terminated disulfides, except that d_3-methyl iodide and ethyl iodide, respectively, were used. Thin-layer chromatography and mass spectrometry verified that each of the disulfide products was pure.

The HO-SAM, CH_3O-SAM, CD_3O-SAM, and CH_3CH_2O-SAM surfaces bound to gold films through sulfur linkages, $HO(CH_2)_{11}S$-Au, $CH_3O(CH_2)_{11}S$-Au, $CD_3O(CH_2)_{11}S$-Au, and $CH_3CH_2O(CH_2)_{11}S$-Au, respectively, were prepared from the synthesized disulfide products and used as the adsorbates in the ion/surface scattering experiments. Substrates were prepared by thermal evaporation of 100 Å of chromium then 2000 Å of gold onto silicon wafers of orientation ⟨1 0 0⟩ (International Wafer Service, Portola Valley, CA). The molecular assemblies were constructed by immersing the substrates into 5 mM ethanol solutions of the disulfides for at least 1 week. In addition, a series of mixed monolayer surfaces was prepared by mixing different amounts of two of the disulfides in ethanol, the total concentration of the two being about 5 mM. Each of the surfaces was allowed to assemble in solution for a period of at least 1 week at room temperature. Detailed information concerning the preparation and properties of SAM surfaces has been provided elsewhere [35]. After assembly the surfaces were rinsed and sonicated in ethanol, then dried under argon before being introduced into the high-vacuum scattering chamber.

2.2. Ion/surface scattering experiments

All experiments were performed in a custom-built, hybrid mass spectrometer with geometry BEEQ (B = magnetic sector, E = electric sector, Q = quadrupole mass analyzer), a detailed description of which has been provided [36]. Briefly, volatile samples were independently introduced into the ion source (10^{-5} Torr nominal sample pressure) and ionized by electron impact (70 eV). Ions of interest were accelerated to ca. 2 keV translational energy and mass and energy selected, respectively, by the magnetic and electrostatic analyzers of the double focusing mass spectrometer. Projectile ions of interest were decelerated to low translational energies (<100 eV), then allowed to collide with the surface in a high-vacuum scattering chamber maintained at a nominal base pressure of 2×10^{-9} Torr (typical operating pressures were below 5×10^{-9} Torr).

For the ion/surface scattering experiments, the sample was rotated so that the primary ion beam was incident at 55° to the surface normal, while scattered ions were collected at approximately the specular angle. Collection angles were not varied, but ion trajectory simulations show that under the conditions used, the analytical system accepts a wide range of scattering angles, approximately 30° on either side of the specular angle. Scattered ions were analyzed using a quadrupole mass analyzer preceded by an electrostatic analyzer, used as a kinetic energy to charge filter. The kinetic energy analyzer was set in a low-resolution mode so as to pass ions of a broad range of energies in the range of a few eV. These conditions are known to efficiently transfer the products of inelastic, reactive, and chemical sputtering processes [36]. The selected conditions give maximum scattered ion transmission without significant angular or velocity discrimination, although the latter types of experiments have been performed earlier, using the same instrumentation. Projectile ions used in this study were CF_3^+, $SiCl_3^+$, and $C_5H_5N^{\bullet+}$. These were derived, respectively, from electron ionization of *n*-perfluorohexane, silicon tetrachloride, and pyridine (Aldrich Inc.).

3. Results and discussion

3.1. Overview of ion/surface collision processes at CH_3O-SAM surfaces

The projectile ions, CF_3^+, $SiCl_3^+$, and $C_5H_5N^{\bullet+}$, were collided with the CH_3O-SAM surface at collision energies ranging from 25 to 80 eV. The scattered ions can be categorized as being the products of elastic scattering, dissociative scattering, reactive scattering, or chemical sputtering. The combined ion abundances in each group have been normalized for each collision energy and expressed in the form of an energy-resolved mass spectra (ERMS) plot, as shown in Fig. 1. This figure for the methoxy-terminated surface compares the normalized abundance of scattered ions due to each of the four process types for the various projectiles. From the ERMS plot shown in Fig. 1a, which represents scattered ion mass spectra derived from collisions of the pyridine molecular ion, $C_5H_5N^{\bullet+}$, with the CH_3O-SAM surface, it is evident that the most abundant ions observed in the mass spectra are reactively and dissociatively scattered. Reactive scattering is the most important scattering process at collision energies below 35 eV and is largely associated with H atom abstraction from the surface by the projectile radical cation. Hydrogen atom abstraction, which is represented by formation of the $(M+H)^+$ ion, has previously been shown to be a favorable reaction [37] for odd-electron ions impinging on hydrocarbon surfaces. As the collision energy is increased, more energy is transferred into the internal coordinates of both the reactively scattered $(M+H)^+$ product and the (in)elastically scattered $M^{\bullet+}$ ion, and both of these ions undergo fragmentation. The dissociatively scattered (SID) product ions dominate the secondary ion mass spectra at higher collision energies. Chemically sputtered ions originating from

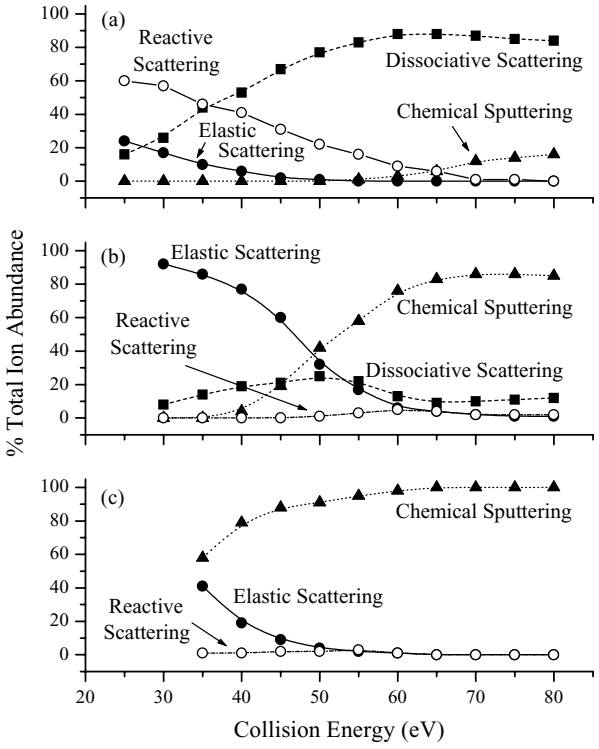

Fig. 1. Energy-resolved mass spectra (ERMS) plot recorded upon scattering (a) $C_5H_5N^{\bullet+}$, (b) $SiCl_3^+$, and (c) CF_3^+ from a CH_3O-SAM surface over a collision energy range, 25–80 eV.

the surface are also observed at higher collision energies but comprise only a small proportion of the scattered ion mass spectra. It has been shown previously that the two ion/surface collision processes of most interest here, SID and a particular type of ion/surface reactive scattering, viz. H atom abstraction, are influenced by the chemical nature of the surface adsorbates [11,38]. Therefore, since these processes are favorable for collisions involving the $C_5H_5N^{\bullet+}$ ion and yield intense ion signals, measurement of those signals allows ready differentiation of adsorbates at surfaces.

Fig. 1b illustrates the ERMS plot derived from experimental data on collisions of the $SiCl_3^+$ ion with the CH_3O-SAM surface over a range of collision energies. The increased stability and lower reactivity expected of an even-electron ion like $SiCl_3^+$ is evident in the much greater importance of elastic scattering and the reduced importance of reactive scattering in the ERMS plot compared with that for pyridine molecular ion collisions. Abstraction of atoms or groups of atoms from the surface is observed, accompanied by dissociation of the $SiCl_3^+$ ion. These ion/surface dissociative reactions, though minor processes for this ion, are important because they reveal the identity of functional groups at the surface. Another significant difference between the ERMS plot of $SiCl_3^+$, in comparison to that of the molecular ion of pyridine, is the large abundance of chemically sputtered ions and the relatively low abundance of dissociatively scattered ions observed at higher collision energies. These differences are attributed to the preference of $SiCl_3^+$ to undergo charge exchange. Using known gas-phase energetics, the recombination energy of $SiCl_3^+$ is calculated to be 11.0 eV [39], while that for pyridine is 9.3 eV [40]. The former value suffices for ionization of the adsorbate, whose ionization energy in various estimates ranges from 9.3 to 10.3 eV [39], while the latter does not. The reaction products observed at higher collision energies, along with the chemically sputtered ions, both generated upon collision of the $SiCl_3^+$ ion with the CH_3O-SAM surface, are the processes of interest for surface analysis.

Fig. 1c illustrates the ERMS plot derived from collisions of the CF_3^+ ion with the CH_3O-SAM surface. The plot shows that chemically sputtered ions dominate the scattered ion mass spectra, even at collision energies as low as 40 eV. The main difference between the CF_3^+ and $SiCl_3^+$ ions is that essentially no dissociatively scattered or reactively scattered ions are observed in the scattered ion mass spectra acquired as a result of collisions of CF_3^+. Therefore, chemically sputtered ions are the only ions observed at higher collision energies. This preference of CF_3^+ to cause chemical sputtering cannot be accounted for by the value of the recombination energy alone, ~9.8 eV [41]. Rather, the lack of C–F bond activation, and therefore no observation of dissociatively or reactively scattered ions, can be simply attributed to the strength of the C–F bond (bond enthalpy ~ 490 kJ/mol), versus the Si–Cl bond (bond enthalpy ~ 402 kJ/mol) [42]. The dominance of chemically sputtered ions at higher collision energies makes this ion an excellent candidate as a sputtering agent for the chemical analysis of surfaces, and it has indeed been widely used for this purpose [16,43].

3.2. Ion/surface processes occurring upon scattering CF_3^+ from different surfaces

The mass spectrum resulting from the scattering of CF_3^+ ions from an HO-SAM surface at a collision energy of 70 eV is represented in Fig. 2a. Each of the chemically sputtered ions, H_3O^+ (*m/z* 19), CH_2OH^+ (*m/z* 31) and $C_2H_4OH^+$ (*m/z* 45) provide evidence of the terminal hydroxyl functionality present at the monolayer surface. Other ions sputtered from the surface occur at nominal masses that correspond to $C_nH_{2n-1}^+$ and $C_nH_{2n+1}^+$, for example *m/z* 15, 27, 29, 41, and 43. These common fragment ions stem from adventitious hydrocarbon molecules physically adsorbed to the surface. Notice that the elastically scattered ion, CF_3^+, and the dissociatively scattered ions, $CF_2^{\bullet+}$ and CF^+, are not present in this mass spectrum. (Here as elsewhere, the term elastically scattered is used to include quasi-elastically scattered ions, viz., ions that acquire internal excitation but insufficient to cause dissociation on the time scale of the experiment.)

The scattered ion mass spectrum acquired from 70 eV collisions of the CF_3^+ ion with an ether adsorbate, the CH_3O-SAM surface, is shown in Fig. 2b. The most abundant ions in this mass spectrum are observed at *m/z* 15 and 45. These peaks represent the chemically sputtered ions, CH_3^+

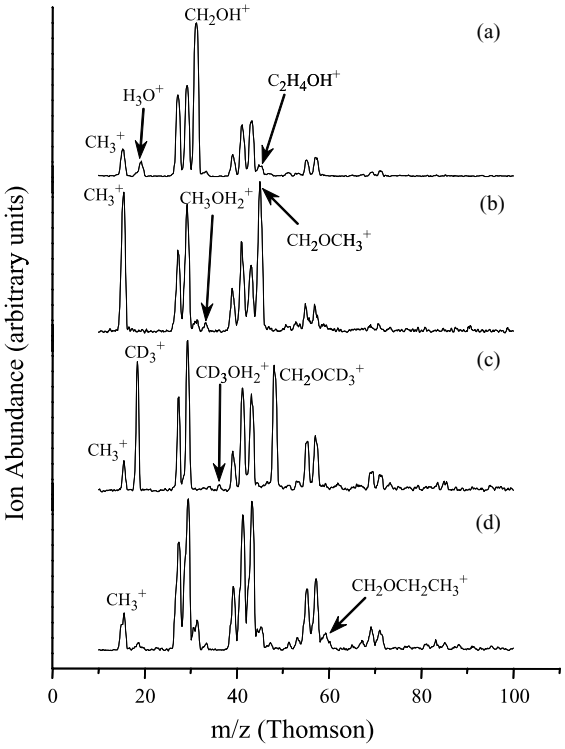

Fig. 2. Scattered ion mass spectra recorded upon 70 eV collisions of CF_3^+ with (a) an HO-SAM surface, (b) a CH_3O-SAM surface, (c) a CD_3O-SAM surface, and (d) a CH_3CH_2O-SAM surface.

and $CH_2OCH_3^+$, both derived from the adsorbate by expected bond cleavages. A minor product, due to chemical sputtering and involving the terminal-OCH_3 group, is the rearrangement fragment, $H_2OCH_3^+$ (*m*/*z* 33), a well-known species in the low-energy electron impact spectra of alkyl ethers [44]. An important observation can be made, here, about the chemical sputtering process. The most abundant ion from the HO-SAM surface, CH_2OH^+, and the most abundant ion from the CH_3O-SAM surface, $CH_2OCH_3^+$, both occur as a result of cleavage of the C–C bond alpha to the oxygen atom. The typical dissociation pathway for molecular ions formed from ethers or alcohols upon ionization by electron impact is also due to C–C cleavage of the alpha bond. Dissociation of gas-phase ions after electron impact ionization and that of surface molecules by chemical sputtering both occur as a result of energetic charge exchange [14], and therefore the same principle which governs the fragmentation of ions generated through electron impact is expected to hold true for the chemical sputtering of fragment ions from surfaces. The scattered ion mass spectrum resulting from 70 eV collisions of CF_3^+ with the CD_3O-SAM surface is shown in Fig. 2c. Isotopic labeling of the methoxy-terminated SAM surface verifies the nature of the sputtered ions observed in Fig. 2b. Chemically sputtered ions characteristic of this deuterated surface include CD_3^+ (*m*/*z* 18), $H_2OCD_3^+$ (*m*/*z* 36), and $CH_2OCD_3^+$ (*m*/*z* 48).

Fig. 2d illustrates scattering of 70 eV CF_3^+ ions from a CH_3CH_2O-SAM surface. The alpha cleavage product, $CH_2OCH_2CH_3^+$ (*m*/*z* 59), is observed in this mass spectrum, as in the previous cases although in relatively low abundance. In its place one observes fragment ions originating by cleavages occurring closer to the terminus of the surface adsorbate, such as $C_2H_3^+$ (*m*/*z* 27) and $C_2H_5^+$ (*m*/*z* 29) in greater abundance. Unlike the situation involving dissociation of ions in the gas phase, the orientation of surface molecules is fixed. Therefore, the fragment corresponding to the energetically favored alpha cleavage, the $CH_2OCH_2CH_3^+$ ion might be generated, but steric constraints appear to allow it to re-bind to the surface and not to be released into the gas phase. This helps explain why chemical sputtering is sensitive to only the outermost two or three atomic layers of a surface.

Since chemically sputtered ions characteristic of the HO-SAM and CH_3O-SAM surfaces are abundant and have different mass-to-charge values, determination and relative quantitation of these two adsorbates on the same surface is possible. Several mixed SAM surfaces were prepared by varying the relative concentrations of the HO-terminated dialkyl disulfide and the CH_3O-terminated dialkyl disulfide in solutions of ethanol. Studies involving the coadsorption of thiols or disulfides on surfaces have shown that the distribution of these molecules across a surface is uniform and does not lead to significant phase segregation, provided the two components are relatively similar in terms of chain length and in dipole moment [45]. From studies involving mixtures of HO- and CH_3-terminated long-chain thiols, it has been shown that solution concentration accurately reflects the assembled surface composition [46], and their coadsorption leads to homogenously mixed SAMs on the micrometer-scale [47]. Scattered ion mass spectra were recorded upon collisions of 70 eV CF_3^+ ions with a series of mixed HO-/CH_3O-terminated SAM surfaces. The chemically sputtered ions derived from the HO-terminated adsorbates, as identified in the previous studies of the pure adsorbates, are reported as a fraction of the total amount of chemically sputtered ions (i.e., those derived from both the HO-terminated and CH_3O-terminated molecules). These percentages were plotted versus the percent of HO-terminated molecules present in the solution and the results are shown in Fig. 3. The relationship between the two is non-linear. For the solution containing 60% HO-terminated and 40% CH_3O-terminated molecules, the percent of chemically sputtered ions derived from the HO-terminated adsorbate is less than 20% of the total. Preferential sputtering of the CH_3O-terminated adsorbate molecules is evident.

To demonstrate that this result is an effect of the chemical sputtering event, mixed SAM surfaces were prepared by coadsorption of the CH_3O-terminated molecules with the CD_3O-terminated molecules. Scattered ion mass spectra were recorded upon collision of 70 eV CF_3^+ ions with a series of mixed CH_3O-/CD_3O-terminated SAM surfaces. The chemically sputtered ions derived from the

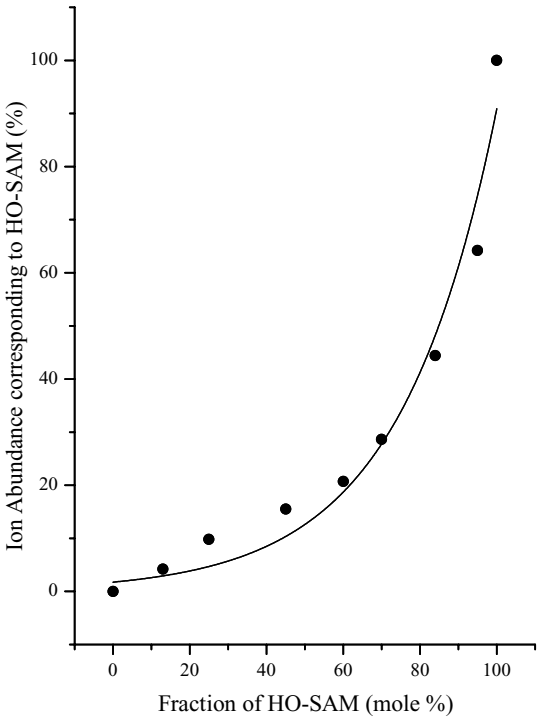

Fig. 3. Chemically sputtered ions observed in the CF_3^+ scattered ion mass spectra that originate from HO-terminated molecules reported as a fraction of the total amount of chemically sputtered ions, arising from both the HO-terminated and CH_3O-terminated molecules. These fractions are plotted against a series of mixed SAM surfaces, for which the percentage of HO-terminated dialkyl disulfide in the assembling solution was varied. The line drawn through the data is not representative of a trend, but is useful for visualization of the data.

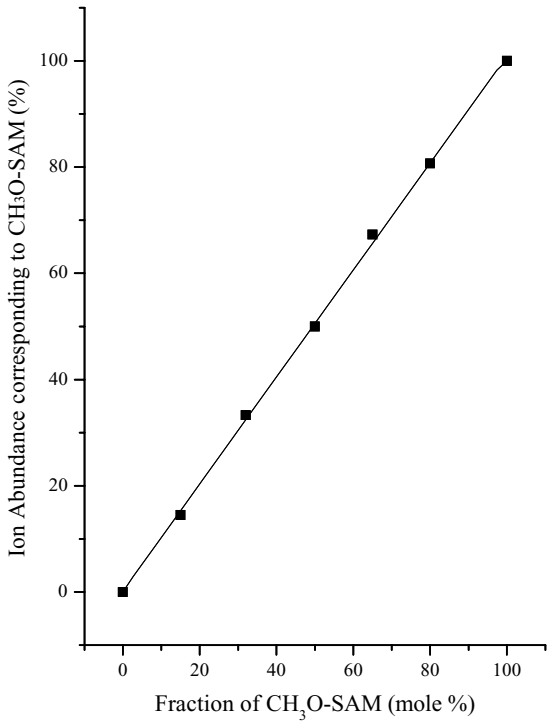

Fig. 4. Chemically sputtered ions observed in the CF_3^+ scattered ion mass spectra that originate from CH_3O-terminated adsorbates are reported as a fraction of the total amount of chemically sputtered ions, arising from both the CH_3O-terminated and CD_3O-terminated adsorbates. These fractions are plotted for a series of mixed SAM surfaces, for which the percentage of CH_3O-terminated dialkyl disulfide in the assembling solution was varied. A regression line fits the data.

CH_3O-terminated adsorbates are reported as a fraction of the total number of chemically sputtered ions (i.e., those derived from both the CH_3O-terminated and the CD_3O-terminated adsorbate molecules). These percentages were plotted against the percent of CH_3O-terminated molecules present in the solution and the data are shown in Fig. 4. This graph shows the expected 1-1 linear relationship. For the solution containing 50% CH_3O-terminated molecules and 50% CD_3O-terminated molecules, the proportion of chemically sputtered ions derived from the CH_3O-terminated adsorbates and observed in the CF_3^+ scattered ion mass spectrum is 50% of the total.

Preferential sputtering of the methoxy-terminated adsorbate in comparison to the hydroxy-terminated adsorbate might be explained by the relative thermochemistry of the two events. Small molecules with functional groups representative of these adsorbates are 1-propanol, $CH_3CH_2CH_2OH$, and ethyl methyl ether, $CH_3CH_2OCH_3$. Bowen and Maccoll showed that the ionization energy of 1-propanol (10.2 eV) is larger than the ionization energy of ethyl methyl ether (9.7 eV) [48] and perhaps more significantly, even more different from the recombination energy of the projectile ion, CF_3^+, ~9.8 eV [41]. Furthermore, the appearance energy of CH_2OH^+ from 1-propanol (12.3 eV) is greater than the appearance energy of $C_2H_4OH^+$ from ethyl methyl ether (10.5 eV). These gas-phase ion energetic data show that chemical sputtering of the methoxy-terminated adsorbate is thermodynamically more favorable than that of the hydroxy-terminated adsorbate. It is also possible that the difference in the length of the two adsorbates also contributes to the observed preferential sputtering. The larger methoxy-terminated adsorbate may hinder access to the HO-terminated adsorbates, making charge exchange between the impinging ion and the methoxy group more likely. The selectivity of chemical sputtering for the outermost portions of a surface has already been demonstrated by the chemical sputtering results from the CH_3CH_2O-, CH_3O-, and HO-terminated surfaces. The non-linear results in Fig. 3 and therefore the preferential chemical sputtering of the methoxy-terminated adsorbate in comparison to the hydroxy-terminated adsorbate are attributed to the favored thermochemistry and the greater extension of the CH_3O-terminated adsorbates from the gold.

3.3. Ion/surface processes occurring upon scattering of the molecular ion of pyridine from different surfaces

Fig. 5a shows the scattered ion mass spectrum resulting from 30 eV collisions of the molecular ion of pyridine,

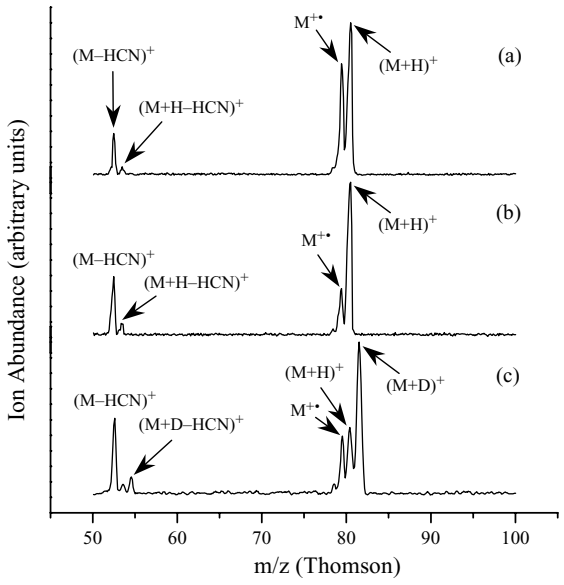

Fig. 5. Scattered ion mass spectra were recorded upon 30 eV collisions of $C_5H_5N^{\bullet+}$ with (a) an HO-SAM surface, (b) a CH_3O-SAM surface, and (c) a CD_3O-SAM surface.

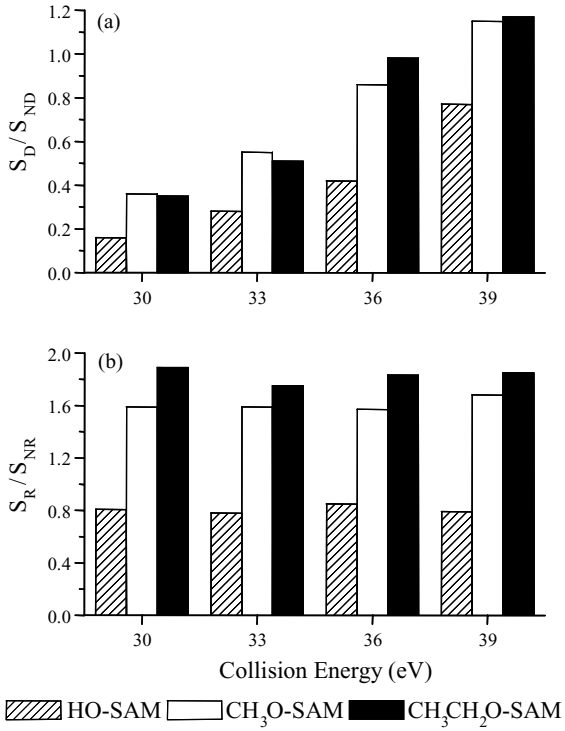

Fig. 6. (a) Ratio of the peak intensities arising from dissociatively scattered ions (S_D) plotted against the peak intensities arising from non-dissociatively scattered ions (S_{ND}) for mass spectra showing scattering of the molecular ion of pyridine from the HO-SAM, CH_3O-SAM, and CH_3CH_2O-SAM surfaces over the collision energy range 30–40 eV. (b) Ratio of peak intensities arising from reactively scattered ions (S_R) plotted against the peak intensities arising from the non-reactively scattered ions (S_{NR}) for mass spectra resulting from the scattering of the molecular ion of pyridine from the HO-SAM, CH_3O-SAM, and CH_3CH_2O-SAM surfaces over the collision energy range 30–40 eV.

$C_5H_5N^{\bullet+}$, from a HO-SAM surface. The elastically scattered $M^{\bullet+}$ ion (*m/z* 79) is abundant at this collision energy, as is the reactively scattered $(M+H)^+$ ion (*m/z* 80). Dissociatively scattered ions include the $(M-H)^+$ fragment ion (*m/z* 78), the $(M-HCN)^+$ ion (*m/z* 52), and the $(M+H-HCN)^+$ ion (*m/z* 53). The same ions are observed in Fig. 5b, which displays the scattered ion mass spectrum resulting from 30 eV collisions of $C_5H_5N^{\bullet+}$ with the CH_3O-SAM surface. The only difference from Fig. 5a is the relative intensities of these peaks. Note that in Fig. 5a, the H abstraction product is more abundant than the $M^{\bullet+}$ ion while in Fig. 5b it is several times more abundant than $M^{\bullet+}$, which is consistent with the greater density of surface hydrogen atoms. Fig. 5c shows the scattered ion mass spectrum resulting from 30 eV collisions of $C_5H_5N^{\bullet+}$ with a CD_3O-SAM surface. With D atoms available for abstraction, the expected $(M+D)^+$ ion (*m/z* 81) is observed as well as the dissociation product of that ion $(M+D-HCN)^+$ (*m/z* 54). Notice, however, that the $(M+H)^+$ ion (*m/z* 80) is also present, in approximately one-half the abundance of the D atom abstraction product. Previous studies have shown that H atom abstraction from underlying atomic layers of a monolayer surface is not a favored event. Rather, the observed H atom abstraction is more likely to occur from reaction with adventitious hydrocarbon. Note that the presence of hydrocarbon molecules is observed in the CF_3^+ scattered ion mass spectra as well (Fig. 1). The relative abundance of the molecular ion in comparison to the reactively scattered and dissociatively scattered products is similar for the CD_3O-SAM and CH_3O-SAM surfaces, a further demonstration that the differences observed in the scattering of $C_5H_5N^{\bullet+}$ from the HO-SAM and CH_3O-SAM surfaces are due to chemical effects. These differences can be explained either by increased energy transfer at the CH_3O-SAM surface or increased reactivity. Both factors are likely to contribute.

A more detailed analysis of these results is provided by considering collisions of the $C_5H_5N^{\bullet+}$ ion with the HO-SAM, CH_3O-SAM, and CH_3CH_2O-SAM surfaces in the collision energy range, 30–40 eV. The two graphs shown in Fig. 6 isolate the processes which create the observed differences in the scattered ion mass spectra collected on collision of the $C_5H_5N^{\bullet+}$ ion with the oxygenated SAM surfaces. Fig. 6a reports the measured ratio, S_D/S_{ND}, where S_D is the sum of all fragment ions observed in the mass spectra, and S_{ND} is the sum of all ions observed in the mass spectra which do not involve fragmentation. Effectively this ratio is a rough measure of the internal energy transferred to the projectile ion upon collision with each of the surfaces. The fragment ions arise from the molecular radical cation and the protonated molecule—the major precursor ions. The graph shows that over the collision energy range, 30–40 eV, the relative abundance of the molecular ion is lower for the CH_3O-SAM and the CH_3CH_2O-SAM surfaces than for the HO-SAM surface. The greater tendency of the former two surfaces for hydrogen abstraction will certainly contribute to the result together with the effect of energy transfer. No

consistent differences were observed upon comparison of the CH_3O-SAM and CH_3CH_2O-SAM surfaces.

Fig. 6b reports the measured ratio, S_R/S_{NR}, where S_R is the sum of all ions observed in the mass spectra which undergo reaction with the surface (this includes both the $(M+H)^+$ and $(M+H-HCN)^+$ ions), and S_{NR} is the sum of all ions observed in the mass spectra which do not react with the surface. In effect, this graph measures the reactivity of the $C_5H_5N^{\bullet+}$ ion upon interaction with each of the surfaces. The results from this graph show that the order of H atom abstraction reactivity from least to greatest is HO-SAM < CH_3O-SAM < CH_3CH_2O-SAM. The reactivity trend observed in Fig. 6b likely stems from the greater availability of H atoms at the CH_3O-SAM surface than at the HO-SAM surface.

3.4. Ion/surface processes occurring upon scattering of $SiCl_3^+$ from different surfaces

Fig. 7a illustrates the scattered ion mass spectrum recorded upon 60 eV collisions of $SiCl_3^+$ with an HO-SAM surface. Note that each of the ion/surface collision processes discussed in Sections 3.1–3.3 leads to representative ions in this mass spectrum. The elastically scattered $SiCl_3^+$ ion (*m/z* 133) is present as are the inelastically scattered ions, $SiCl_2^{\bullet+}$ (*m/z* 98) and $SiCl^+$ (*m/z* 63). In addition, the same chemically sputtered ions observed in the scattering of the CF_3^+ ion from this surface, are observed, namely H_3O^+ (*m/z* 18), CH_2OH^+ (*m/z* 31), and $C_2H_4OH^+$ (*m/z* 45). The unique contribution made to surface analysis by this ion involves the presence of the many ion/surface reaction products. These reaction products include $SiClH_2^+$ (*m/z* 65), $SiClO^+$ (*m/z* 79), $SiClH(OH)^+$ (*m/z* 81), $SiCl(OH)_2^+$ (*m/z* 97), $SiCl_2H^+$ (*m/z* 99), and $SiCl_2OH^+$ (*m/z* 115). Abstraction of chemical groups from the surface by the $SiCl_3^+$ ion to form scattered ion products of the form, $SiCl_3X^{\bullet+}$, is a thermodynamically unfavorable event, but dissociation of $SiCl_3^+$ at the surface provides opportunities for the addition of other atoms or groups of atoms. (For example, the former reaction with H-SAM is estimated to have a higher reaction enthalpy than the latter by ca. 20 kcal/mol.) These dissociative ion/surface reaction products are indicative of the groups present at the surface. The scattered ion mass spectrum resulting from 60 eV collisions of the $SiCl_3^+$ ion with the CH_3O-SAM surface is shown in Fig. 7b. The chemically sputtered ions are the same as those observed in the CF_3^+ scattered ion mass spectra, namely CH_3^+ (*m/z* 15) and $CH_2OCH_3^+$ (*m/z* 45). However, the presence of the OCH_3 group at this surface is confirmed through observation of the ion/surface reaction products. These ions include $SiClH_2^+$ (*m/z* 65), $SiClH(CH_3)^+$ (*m/z* 79), $SiClH(OCH_3)^+$ (*m/z* 95), $SiCl_2H^+$ (*m/z* 99), $SiCl_2CH_3^+$ (*m/z* 113), and $SiCl_2OCH_3^+$ (*m/z* 129). Several of these products are confirmed by the isotopic data shown in Fig. 7c, which illustrates the scattered ion mass spectrum resulting from 60 eV collision of $SiCl_3^+$ with a CD_3O-SAM surface. Fig. 7d illustrates the scattered ion mass spectrum resulting from 60 eV collisions of the $SiCl_3^+$ ion with the CH_3CH_2O-SAM surface. Ion/surface reaction products were observed that contain alkyl groups from the surface, $SiCl_2CH_3^+$ (*m/z* 113) and $SiCl_2C_2H_5^+$ (*m/z* 127), but no products contained the O atom from the surface. Reaction of the projectiles proves to be limited to the outermost atomic layers of the surface, similar to the results observed from chemical sputtering.

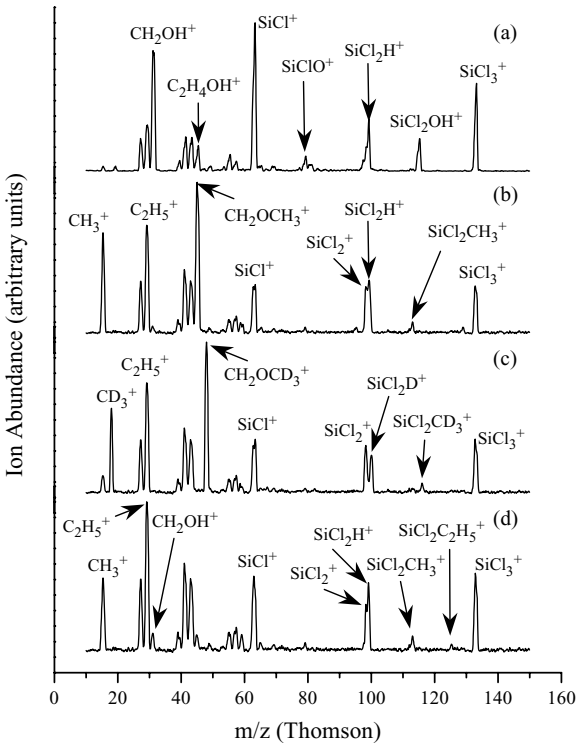

Fig. 7. Scattered ion mass spectra resulting from 60 eV collisions of $SiCl_3^+$ with (a) an HO-SAM surface, (b) a CH_3O-SAM surface, (c) a CD_3O-SAM surface, and (d) a CH_3CH_2O-SAM surface.

4. Conclusion

Differences in the relative amounts of reactively and dissociatively scattered ions observed when 30 eV $C_5H_5N^{\bullet+}$ ions are collided with each of three oxygenated surfaces were used to show that this approach provides many features that allow adsorbates to be characterized, even when they are chemically similar. The order of reactivity for this ion from the least to the greatest is HO-SAM < CH_3O-SAM < CH_3CH_2O-SAM. The relative fragment ion abundance in the SID spectra of $C_5H_5N^{\bullet+}$ ions occurs in the order HO-SAM < CH_3O-SAM ~ CH_3CH_2O-SAM and these two factors might be inter-related. The increased availability of H atoms at the CH_3CH_2O-terminated monolayer surface as compared to the HO-terminated monolayer surface is an alternative explanation which is also consistent with previous results for other systems [38,49].

Collisions involving the CF_3^+ and $SiCl_3^+$ ions gave more specific information about the chemical composition of these surfaces, and they do so through different processes. Scattering with the CF_3^+ ion at 70 eV collision energy yields only chemically sputtered ions. The preferred fragmentation route of these oxygenated adsorbate molecules is cleavage of the C–C bond alpha to the oxygen functional group. This preferential bond cleavage provides qualitative and quantitative information about these isomeric surfaces. Scattering of $SiCl_3^+$ ion at 60 eV collision energy yields dissociative ion/surface reaction products, which contain groups or atoms indicative of the functional groups belonging to those surfaces.

In conclusion, this study shows that sensitive, selective chemical information can be derived for adsorbate-covered surfaces using low-energy ion/surface collisions and that this information is specific to the uppermost two or three atomic layers of the adsorbate.

Acknowledgements

This work was supported by the National Science Foundation, CHE-9732670.

References

[1] R.G. Cooks, D.H. Terwilliger, T. Ast, J.H. Beynon, T. Keough, J. Am. Chem. Soc. 97 (1975) 1583.
[2] A.R. Dongre, A. Somogyi, V.H. Wysocki, J. Mass Spectrom. 31 (1996) 339.
[3] R.G. Cooks, Md.A. Mabud, S.R. Horning, X.Y. Jiang, C. Paradisi, P. Traldi, J. Am. Chem. Soc. 111 (1989) 859.
[4] C.G. Gu, V.H. Wysocki, J. Am. Chem. Soc. 119 (1997) 12010.
[5] T. Pradeep, J.W. Shen, C. Evans, R.G. Cooks, Anal. Chem. 71 (1999) 3311.
[6] J.W. Shen, C. Evans, N. Wade, R.G. Cooks, J. Am. Chem. Soc. 121 (1999) 9762.
[7] E.T. Ada, O. Kornienko, L. Hanley, J. Phys. Chem. 102 (1998) 3959.
[8] J. Laskin, E.V. Denisov, J.H. Futrell, J. Am. Chem. Soc. 122 (2000) 9703.
[9] V. Grill, J. Shen, C. Evans, R.G. Cooks, Rev. Sci. Instrum. 72 (2001) 3149.
[10] C.G. Gu, A. Somogyi, V.H. Wysocki, K.F. Medzihradszky, Anal. Chim. Acta. 397 (1999) 247.
[11] M.R. Morris, D.E. Riederer Jr., B.E. Winger, R.G. Cooks, T. Ast, C.E.D. Chidsey, Int. J. Mass Spectrom. Ion Process. 122 (1992) 181.
[12] J.H. Callahan, A. Somogyi, V.H. Wysocki, Rapid Commun. Mass Spectrom. 7 (1993) 693.
[13] C. Mair, M. Lezius, Z. Herman, T.D. Märk, J. Chem. Phys. 118 (2003) 7090.
[14] T. Ast, D.E. Riederer Jr., S.A. Miller, M. Morris, R.G. Cooks, Org. Mass Spectrom. 28 (1993) 1021.
[15] M. Vincenti, R.G. Cooks, Org. Mass Spectrom. 23 (1988) 317.
[16] R.G. Cooks, T. Ast, T. Pradeep, V. Wysocki, Acc. Chem. Res. 27 (1994) 316.
[17] T. Ast, Md.A. Mabud, R.G. Cooks, Int. J. Mass Spectrom. Ion Process. 82 (1988) 131.
[18] R.G. Cooks, T. Ast, Md.A. Mabud, Int. J. Mass Spectrom. Ion Process. 100 (1990) 209.
[19] M.E. Bier, J.C. Schwartz, K.L. Schey, R.G. Cooks, Int. J. Mass Spectrom. Ion Process. 103 (1990) 1.
[20] E.R. Williams, G.C. Jones Jr., L. Fang, R.N. Zare, B.J. Garrison, D.W. Brenner, J. Am. Chem. Soc. 114 (1992) 207.
[21] C. Evans, T. Pradeep, J. Shen, R.G. Cooks, Rapid Commun. Mass Spectrom. 13 (1999) 172.
[22] B. Feng, J. Shen, V. Grill, C. Evans, R.G. Cooks, J. Am. Chem. Soc. 120 (1998) 8189.
[23] N. Wade, J. Shen, J. Koskinen, R.G. Cooks, J. Mass Spectrom. 36 (2001) 717.
[24] T. Pradeep, T. Ast, R.G. Cooks, B. Feng, J. Phys. Chem. 98 (1994) 9301.
[25] U. Mazurek, H. Schwarz, Chem. Commun. 12 (2003) 1321.
[26] T. Pradeep, C. Evans, J.W. Shen, R.G. Cooks, J. Phys. Chem. B 103 (1999) 5304.
[27] N. Wade, T. Pradeep, J.W. Shen, R.G. Cooks, Rapid Commun. Mass Spectrom. 13 (1999) 986.
[28] T. Pradeep, B. Feng, T. Ast, J.S. Patrick, R.G. Cooks, S.J. Pachuta, J. Am. Soc. Mass Spectrom. 6 (1995) 187.
[29] K.H. Park, B.C. Kim, H. Kang, J. Chem. Phys. 97 (1992) 2742.
[30] S.R. Kasi, H. Kang, J.W. Rabalais, J. Chem. Phys. 88 (1988) 5914.
[31] M.B.J. Wijesundara, L. Hanley, B.R. Ni, S.B. Sinnott, Proc. Natl. Acad. Sci. U.S.A. 97 (2000) 23.
[32] N. Wade, B. Gologan, A. Vincze, R.G. Cooks, D.M. Sullivan, M.L. Bruening, Langmuir 18 (2002) 4799.
[33] N. Wade, C. Evans, S.-C. Jo, R.G. Cooks, J. Mass Spectrom. 37 (2002) 591.
[34] C. Evans, N. Wade, F. Pepi, G. Strossman, T. Schuerlein, R.G. Cooks, Anal. Chem. 74 (2002) 317.
[35] C.E.D. Chidsey, D.M. Loiacono, Langmuir 6 (1990) 682.
[36] B.E. Winger, H.-J. Laue, S.R. Horning, R.K. Julian Jr., S.A. Lammert, D.E. Riederer Jr., R.G. Cooks, Rev. Sci. Instrum. 63 (1992) 5613.
[37] T.E. Kane, A. Somogyi, V.H. Wysocki, Org. Mass Spectrom. 28 (1993) 1665.
[38] V.J. Angelico, S.A. Mitchell, V.H. Wysocki, Anal. Chem. 72 (2000) 2603.
[39] M.W. Chase Jr., NIST-JANAF Thermochemical Tables, 4th ed., Springer-Verlag, Inc., New York, 1998, p. 1951.
[40] C. Lifshitz, J. Phys. Chem. 86 (1982) 606.
[41] T.C. Ehlert, J. Phys. Chem. 73 (1969) 949.
[42] D.F. Shriver, P.W. Atkins, C.H. Langford, Inorganic Chemistry, 2nd ed., W. H. Freeman & Company, New York, 1994, p. 819.
[43] R. Selvan, D.L. Smith, F. Fernandez, Z. Qi, X. Yang, V.H. Wysocki, Abstracts of Papers, 225th ACS National Meeting, New Orleans, LA, US, 23–27 March 2003.
[44] H. Budzikiewicz, C. Djerassi, D.H. Williams (Ed.), Interpretation of Mass Spectra of Organic Compounds, Holden-Day Inc., San Francisco, 1964, p. 271.
[45] K. Tamada, M. Hara, H. Sasabe, W. Knoll, Langmuir 13 (1997) 1558.
[46] L. Bertilsson, B. Liedberg, Langmuir 9 (1993) 141.
[47] S. Chen, L. Li, C.L. Boozer, S. Jiang, J. Phys. Chem. B 105 (2001) 2975.
[48] R.D. Bowen, A. Maccoll, Org. Mass Spectrom. 19 (1984) 379.
[49] A. Somogyi, D.L. Smith, V.H. Wysocki, R. Colorado Jr., T.R. Lee, J. Am. Soc. Mass Spectrom. 13 (2002) 1151.